UC Irvine
UC Irvine Previously Published Works

Title

NF-κB responds to absolute differences in cytokine concentrations.

Permalink

Journal

Authors

Son, Minjun
Wang, Andrew
Tu, Hsiung-Lin
et al.

Publication Date

DOI

Peer reviewed

NF-κB responds to absolute differences in cytokine concentrations

Minjun Son[1,2], **Andrew G. Wang**[1], **Hsiung-Lin Tu**[1,3], **Marie Oliver Metzig**[4,5], **Parthiv Patel**[1], **Kabir Husain**[6], **Jing Lin**[1], **Arvind Murugan**[6], **Alexander Hoffmann**[4,5], **Sava   Tay**[1,2,*]

[1]Pritzker School of Molecular Engineering, University of Chicago, Chicago, IL 60637, USA.

[2]Institute for Genomics and Systems Biology, University of Chicago, Chicago, IL 60637, USA.

[3]Institute of Chemistry, Academia Sinica, Taipei 11529, Taiwan.

[4]Department of Microbiology, Immunology and Molecular Genetics, University of California, Los Angeles, CA 90095, USA.

[5]Institute for Quantitative and Computational Biosciences, University of California, Los Angeles, CA 90095, USA.

[6]James Franck Institute and Department of Physics, University of Chicago, Chicago, IL 60637, USA.

Abstract

Cells receive a wide range of dynamic signaling inputs during immune regulation, but how gene regulatory networks measure such dynamic inputs is not well understood. Here, we used microfluidic single-cell analysis and mathematical modeling to study how the NF-κB pathway responds to immune inputs that vary over time such as increasing, decreasing, or fluctuating cytokine signals. We found that NF-κB activity responded to the absolute difference in cytokine concentration and not to the concentration itself. Our analyses revealed that negative feedback by the regulatory proteins A20 and IκBα enabled differential responses to changes in cytokine dose by providing a short-term memory of previous cytokine concentrations and by continuously resetting kinase cycling and receptor abundance. Investigation of NF-κB target gene expression showed that cells exhibited distinct transcriptional responses under different dynamic cytokine profiles. Our results demonstrate how cells use simple network motifs and transcription factor dynamics to efficiently extract information from complex signaling environments.

INTRODUCTION

Cells receive temporally varying signals such as cytokines and pathogenic molecules that encode information on the identity, amplitude, and timing of extracellular challenges during the immune response. This information is transmitted into the nuclear localization dynamics of key transcription factors such as nuclear factor κB (NF-κB), which is then decoded by gene regulatory machinery to create specific gene expression responses (1–4). Among those signaling molecules are the central inflammatory cytokines tumor necrosis factor (TNF) and interleukin-1β (IL-1β), which mediate local activation of neighboring cells and coordinate population- and system-level responses. In response to infection in humans and mice, TNF and IL-1β levels in tissue and plasma show a rapid increase and can be sustained at a high level for hours up to many days (5–10). On the other hand, the cytokine levels in the tissue microenvironment can be dynamic (11–13). Individual macrophages and T cells secrete cytokines in complex temporal profiles, such as in pulses and oscillations, in an input-specific manner (14–16). These and other observations have led to the hypothesis that cytokine dynamics and the subsequent proinflammatory responses are connected by a "temporal code" that transmits information from cell surface receptors to gene expression (17).

NF-κB is a key mediator of cytokine signaling and is central to many physiological scenarios in immunity and disease, such as infection, autoimmunity, and cancer. Nuclear translocation of NF-κB family transcription factors such as p65 leads to the activation of nearly 1000 inflammatory and immune response genes (18). Both population-averaged and single cell–resolved measurements show that NF-κB activation discriminates between different doses of signaling molecules including TNF and lipopolysaccharide (4, 19–21). However, it is not known whether cells perceive and respond to the absolute concentration of the cytokine signals independently of past cytokine exposure, as would be the case for a memory-less system, or to the relative changes in cytokine levels because cells can remember previous cytokine levels. Certain biological circuits can store signaling input information in biochemical memory and tailor their response on the basis of prior levels or the "history" of environmental signals. For example, fold-change detection of environmental signals was first described in the chemotaxis of bacteria, where a cellular response is constantly maintained across equal fold changes in chemoattractant concentration (22, 23). Many important eukaryotic signaling pathways in cell growth/differentiation (including extracellular signal–regulated kinase 2, transforming growth factor–β, and Akt), embryonic development, and cancer (such as Wnt) also exhibit fold-change detection to the extracellular ligands (22). However, in the context of infection and inflammation, it is not known how key gene regulatory networks such as NF-κB interpret fluctuating concentrations of extracellular signaling molecules, whether they respond to the absolute cytokine level or to the rate of change.

To address this important question, we studied how mammalian cells respond to dynamically changing cytokine concentrations. Using high-throughput microfluidic live-cell analysis, single-cell tracking, and mathematical modeling, we investigated whether the NF-κB system exploits the temporal characteristics of signals (the input dynamics) during inflammatory signaling. We found that NF-κB dynamics precisely correlated to the rate of change in TNF

and IL-1β, not their absolute levels or to fold changes in concentration. Our theoretical and experimental analyses revealed that multipoint negative feedbacks by A20 and inhibitor of nuclear factor κBα (IκBα) proteins enable this dose differentiation behavior specifically in the NF-κB system in response to TNF and IL-1β.

RESULTS

NF-κB dynamics precisely correlate to the rate of change in TNF and IL-1β concentration

To understand how dynamically varying cytokine concentrations are encoded and decoded by a signaling system, two key questions need to be answered: which attributes of the dynamic signals are detected by the responding pathway and how these attributes regulate the response dynamics. The characteristic response of NF-κB transcription factors to cytokine stimulus is oscillatory. The transcription factor p65 translocates into the nucleus and cycles between the cytosol and nucleus upon cellular exposure to cytokine signals (Fig. 1, A and B) (1, 4). These oscillations can be measured by live-cell microscopy using fluorescent reporters (4). We stimulated NIH/3T3 immortalized mouse embryonic fibroblasts (3T3 cells) expressing the p65-DsRed fusion protein with various dynamic cytokine regiments created by a microfluidic device and analyzed peak height and area under the curve (AUC) of each p65 (NF-κB) localization peak, the two measures of total NF-κB nuclear localization most closely correlated with downstream gene expression (4, 24–26).

To identify the input detection mechanism that is used by NF-κB, we delivered periodically increasing doses of TNF and IL-1β to 3T3 fibroblasts in a microfluidic culture device. Extracellular concentration of both signaling molecules were increased in three different patterns (instant, linear, and exponential) in a controlled manner (Fig. 1C). Individual cells were tracked in real time, and nuclear p65-DsRed levels were recorded by video microscopy. Computer-aided analysis of the videos allowed the extraction of nuclear p65 localization traces for each cell.

When TNF or IL-1β was instantly increased to a high dose (10 or 2.5 ng/ml) and maintained at that level, a strong initial nuclear translocation of NF-κB was observed in all cells within 5 min, reaching its peak at around 25 min (Fig. 1A and movies S1 and S2). However, although the dose was maintained at the same level, the amplitude of subsequent nuclear NF-κB oscillations was diminished to 10 to 30% of the initial peak height. The exponential decay of the NF-κB response under constant cytokine level suggested that the response of the NF-κB system became desensitized to the unchanging input.

When TNF or IL-1β was linearly increased to a high dose (increment of 1 or 0.5 ng/ml every 60 min), we observed sustained oscillations (Fig. 2A and movies S1 and S2). The p65 peaks under both linear ramping of TNF and IL-1β increased and were sustained at a consistent level until ramping was terminated. Total p65 localization, as measured by the AUC of nuclear p65 during each ramping step, stayed constant under linearly increasing cytokine doses. Because of the differences in oscillation characteristics between instantaneous increase and linear stepwise ramping, we studied the NF-κB response under exponentially increasing concentration steps. The cytokine concentration was doubled every

60 min until reaching the maximum level. During exponential ramping, we observed that p65 peaks increased continuously until the final concentration was reached (Fig. 2B and movies S1 and S2). When plotted against the logarithm of input change, the mean AUC for each step fitted precisely to a straight line with a correlation coefficient of ~0.984.

One possible explanation for the desensitization of the NF-κB response is a fold-change detection mechanism, but this mechanism cannot account for our results from linear and exponential ramping experiments. If NF-κB behaved as a fold-change detector, then the height or AUC of successive p65 peaks during linear ramping would decrease sharply because the fold change in the cytokine concentration diminishes in every step. For exponential ramping, on the other hand, the peak heights or AUC would be maintained at a constant level. On the contrary, our data showed constant NF-κB peak heights and AUCs under linear ramping and increasing peak heights and AUCs under exponential ramping. This behavior can be best described as a dose "differentiator," such that NF-κB responds to the log difference in cytokine dose (and not to its absolute level or the fold change), similar to an electronic circuit whose output is proportional to the rate of change of the input level.

Having observed NF-κB behaving as a dose differentiator under specific cytokine ramping conditions, we asked how robustly the differentiation behavior held across variable input dynamics. To investigate how the NF-κB system processes randomly fluctuating cytokine levels, we stimulated cells with different levels of TNF or IL-1β in randomly increasing and decreasing concentrations every 60 min (Fig. 2C and fig. S3C). The AUC of each time interval for each sample was calculated and then plotted against the change of the cytokine level at each step. For all random dynamics that we tested, any decrease in cytokine level resulted in a uniformly sharp decrease in nuclear AUC. However, when cytokine levels increased, the AUC maintained a linear relationship to the log of the input change with a correlation coefficient of ~0.91. Our results thus suggest that the NF-κB system robustly differentiates positive rate of change in the TNF/IL-1β dose regardless of input complexity.

Overall, all our results suggest that the NF-κB is analogous to a rectified differentiator, an electronic circuit that differentiates only the positive change in the current, except that its response is proportional to the logarithm of the input difference. We also found that the differentiator behavior in NF-κB held robustly over a wide range of ramping or exponential growth rates in physiological time scales (0.75 to 10 ng/ml per hour or 6- to 120-min doubling time), further supporting the generality of differentiator behavior under various input dynamics (figs. S1, A to C; S2, A to C; and S3, A to C). Thus, the following simple expression best describes the relationship between the input stimulus and nuclear NF-κB localization amplitude or AUC in single cells, for positive changes in cytokine concentrations ($\Delta C_{\text{cytokine}} > 0$)

$$NF\kappa B \sim \log\left(\Delta C_{\text{cytokine}} + 1\right)$$

Dose differentiation depends on IκB kinase dynamics and multiple negative feedback mechanisms

To understand the molecular mechanism behind dose differentiation, we studied specific properties of the NF-κB regulatory network through mathematical modeling. In unstimulated cells, the majority of NF-κB is in the cytosol, sequestered by IκBα proteins (Fig. 3A). Upon activation by TNF or IL-1β, membrane receptors trigger the ubiquitination and phosphorylation of neutral IκB kinase (IKK_n), posttranslational modification events that transform the kinase into an active conformation (IKK_a) and cause the degradation of IκBα protein. IκBα degradation releases NF-κB for nuclear translocation and triggers the transcription of immune response genes including those encoding its own negative regulators, IκBα and A20. IκBα sequesters nuclear NF-κB and exports the complex out to the cytosol. Coincident with NF-κB translocation, IKK_a undergoes conformational changes and phosphorylation at different sites that disrupt its catalytic activity, leaving it in a refractory state (IKK_i) (24, 27, 28). Dephosphorylation and reformation of the IKK subunits is necessary to adopt the poised state (IKK_n) again. Theoretical studies demonstrated that the cycling rates of IKK conformational change can substantially affect the peak height and dynamics of NF-κB activity (29). If IKK_a remains at a high level after the NF-κB and IκBα complex has been exported, then it triggers degradation of IκBα, initiating another cycle of NF-κB translocation. Another important negative feedback component regulated by nuclear NF-κB is A20, a ubiquitin-editing enzyme that inhibits the activation of IKK and facilitates the inactivation of IKK_a (30–32). Both in vitro and in vivo studies showed that defects in A20 cause prolonged nuclear residence of NF-κB and increased immune activity (33, 34).

To computationally identify possible molecular components or NF-κB subcircuits underlying dose differentiation, we constructed a system of 10 differential equations with 25 parameters (see Materials and Methods in the Supplementary Materials) based on our previously published models of the NF-κB pathway (4, 35). About half of the parameters could be estimated on the basis of the previous experimental work. Then, using the simplex search algorithm (36), the parameter values for the other variables were estimated by fitting the simulated nuclear NF-κB dynamics under three different input ramping patterns (instant, linear, and exponential increase) to the corresponding experimental data (see Materials and Methods in the Supplementary Materials). The simulated nuclear NF-κB trajectory closely captured the differentiator trait of our experimental data. Using this parameter set as a basis, we then evaluated the sensitivity of each parameter to the differentiator behavior through a custom-developed scoring system (Fig. 3B, fig. S4, and Materials and Methods in the Supplementary Materials).

We found that the differentiator behavior was largely unaffected by changes in export and import of NF-κB and IκBα across the nuclear membrane (Fig. 3, A and B, black parameters). The rates associated with IKK conformational change exhibited moderate effects. In contrast, the terms associated with expression of A20 and IκBα proteins showed substantial effects when varied (red parameters). The importance of A20 and IκBα parameters for differentiator behavior could be explained by the dependence of A20 and IκBα on the strength or dose of the previous TNF stimulation, which would provide memory of the previous TNF stimulation by damping the subsequent NF-κB response (Fig.

3C). The high sensitivity of the dose differentiation behavior to A20 is intriguing because this is the only element of the model that is not essential to the canonical NF-κB pathway.

A20 controls IKK cycling that transmits information about TNF dose changes to NF-κB

To more thoroughly examine the role of IKK cycling and A20-mediated negative feedback in dose differentiation, we gradually reduced the production level of A20 in our simulations and studied the effect on NF-κB response (as assessed by nuclear NF-κB and active IKK levels) under different TNF input dynamics. When the TNF level was increased in a stepwise fashion and A20 translation was not perturbed, simulations successfully reproduced nuclear NF-κB amplitudes that corresponded to the change in TNF concentration (Fig. 4A). However, when the translation rate of A20 was reduced to a quarter of its natural rate, we found that NF-κB localization did not track with changes in TNF input, thus indicating a disruption in differentiator behavior. In this system, it took longer for the IKK_a level to return to baseline (Fig. 4B, blue curves), decreasing the level of IKK_n available to respond when the next stimulus came. Consequently, IKK_a production in the next input increase did not fully reflect the increase in the TNF input dose, resulting in a damped response to input change. This effect became more pronounced if A20 was removed completely (Fig. 4C), and NF-κB did not accurately reflect the increases in TNF dose. Because IL-1β signaling shares the IKK module and also controls downstream expression of A20, the same A20-dependent mechanism likely explains differentiator behavior under dynamic IL-1β stimulus, although the range of dose or sensitivity would be different because of the difference in receptors and their associated cytosolic complexes.

Hence, the deletion of A20 results in two key outcomes: loss of feedback from nuclear NF-κB that transmits information about the previous cytokine dose and longer adaptation time for IKK cycling to return to the ready state to reflect the change in the dose. The first outcome would result in stronger NF-κB responses at lower doses of TNF and earlier saturation of the NF-κB response during input ramping. The second outcome would lengthen the oscillation period for both IKK conformation and NF-κB translocation cycling. These anticipated outcomes of A20 deletion were in cells deficient in A20 (Fig. 5A). To further confirm the longer relaxation time in cells deficient in A20, we continuously stimulated both wild-type background (designated as "empty vector") and A20 knockout cells with a constant dose of TNF. Whereas cells with A20 completed the initial cycle within 60 min of stimulation, the nuclear NF-κB level of A20 knockout cells was still decreasing after 120 min (Fig. 5B). To assess how A20 affects the oscillatory behavior at the single-cell level, we applied a Fourier transformation to each trace to evaluate power spectrum and reveal the most prominent oscillatory frequency in each cell (Fig. 5B). In cells lacking A20, the mean frequency of the oscillations was decreased by more than half, and more power was allocated to the zero frequency (meaning, the non-oscillatory response), demonstrating disruption of oscillatory NF-κB behavior.

Both exponential ramping and constant-dose experiments suggested the critical role of A20 in generating prompt responses to changes in TNF input. To further confirm this notion, we delivered different doses of TNF in random order to A20 knockout cells (Fig. 5C), similar to what we did with wild-type cells (Fig. 2C). Not only did the response to input

change become noisier (with a correlation coefficient of ~0.76, compared to ~0.91 for the wild type), but also a substantial amount of NF-κB remained in the nucleus even after the input level decreased, indicating the system's reduced sensitivity to input dynamics. Last, to confirm that the behavior of our simulated A20 knockout mutant was not biased by initial fitting with the full NF-κB circuit (Fig. 4A), we directly obtained the experimental best fit from the A20 knockout model (fig. S5A). Even after fitting the model without A20 directly, the resulting nuclear NF-κB traces did not reproduce the traces observed from the different ramping experiments. Likewise, the best fit without IKK cycling also failed to reproduce the experimental results (fig. S5B). Hence, both our theoretical and empirical studies demonstrate the importance of A20 in resetting the IKK dynamics and receptor levels.

Although we focused our analysis on the role of A20 in the differentiator behavior under TNF stimulation, it is important to note that both negative feedback mechanisms involving IκBα and A20 are required for the differentiator behavior. Without IκBα, the oscillatory response by NF-κB would not be possible in the first place, and stronger NF-κB activation would require greater IκBα production to remove NF-κB from the nucleus and allow the system to adapt. Our simulation for IκBα level in each ramping case suggested that the trace for IκBα level closely followed that of the NF-κB response in wild-type cells (fig. S7A). However, when A20 was depleted, the production of IκBα was disrupted because of the continuous degradation of IκBα downstream of active TNF receptor, resulting in active IKK (fig. S7B). Hence, coordination of both negative feedback mechanisms acting on multiple points in the signal transduction cascade enables accurate assessment of the input dynamics to produce appropriate NF-κB responses. Although the roles of both negative feedbacks in NF-κB regulation were explored in previous studies, such differentiation capability from the negative feedbacks has not been reported before.

Differentiation is reproduced at the single-cell level

Our study so far suggested that the "mean" NF-κB response corresponded to the change in the TNF and IL-1β dose. However, mean and single-cell behavior can diverge considerably in NF-κB signaling (4, 35). Whether single-cell behavior also reflects differentiation capability has not been explored yet. To examine whether the differentiator behavior of the system persists at the single-cell level, we grouped each single-cell trace from the exponential TNF and IL-1β ramping into four different clusters using agglomerative hierarchical clustering in MATLAB (fig. S8, A and B). To evaluate the differentiator behavior of each cluster, the AUC at each ramping step was calculated for the mean trace and was fitted to a linear line (fig. S8, A and B, thick gray line). Each group exhibited some variation due to stochastic activation and/or interactions among molecules involved in the regulation. However, most cells exhibited continuous oscillations and generally increasing peak heights. Although the oscillatory peaks in some groups fluctuated around the fitted lines, the slope of the fitted line in each group was all positive with its y intercept close to zero, which suggests that differentiation is a consistent and reproducible behavior at the single-cell level.

Then, we tried to analyze the source of different group behavior or the fluctuation around the fitted line existing in some groups. During exponential TNF ramping, the majority (~55%) of cells successfully differentiated dose changes at the single-cell level (fig. S8A, group 2). However, a substantial minority of the cells (~23%, group 4) exhibited an interesting behavior: After strong activation in the middle of ramping, NF-κB responses suddenly dropped almost by half, followed by gradual increase thereafter. Although the drop was less pronounced, groups 3 and 4 undergoing exponential IL-1β ramping also exhibited a similar trend in responses. We hypothesized that the stochastic expression of negative feedback elements can explain such behavior in a simple manner. Although the mean behavior exhibits differentiator behavior, transcriptional bursting of downstream negative feedback or different expression capability of cells would cause divergence from the differentiator behavior, leading to fluctuating response around the mean (37, 38). In our simulation, when the transcription rate of the molecules that mediate negative feedback mechanisms was increased, the overall NF-κB response slightly decreased but still demonstrated clear differentiator behavior (fig. S9, A and B, blue lines). When the transcription rate was decreased, the NF-κB response increased sharply for the early period of ramping because of slower production of IκBα and A20 (fig. S9, A and B, red lines). However, the slower production of molecules that mediate negative feedback mechanisms also extended the time required for NF-κB system to adapt to new input dose. If the change in input dose happens before the IKK module completes its cycle, then the system can no longer reflect the increase in input dose, resulting in decreased maximal response. Hence, the decreased production of A20 and/or IκBα due to noisy gene expression can explain the sudden drop observed in a subpopulation of cells.

Dose differentiation is unique to the NF-κB pathway and to cytokine signals

Because inflammatory signaling is complex, with each inflammatory signal acting on multiple systems, we then considered whether TNF and IL-1β dose differentiation is a unique characteristic specific to NF-κB system or a trait common to other regulators that can be induced by these ligands. Although we demonstrated that negative feedbacks downstream of NF-κB are responsible for TNF dose differentiation, the upstream signaling pathway may still have a system associated with the dose differentiation (39). It is also possible that A20 or other negative feedbacks present in other regulatory systems may facilitate the differentiation in those systems. Studying this question would facilitate our understanding of the difference between NF-κB and other systems and would also provide additional evidence for our suggested mechanism for the differentiator behavior.

To investigate the specificity of the differentiator behavior in the NF-κB system, we used the NF-κB and c-Jun N-terminal kinase (JNK) dual reporter 3T3 cell (40–42). JNK is an important kinase in the mitogen-activated protein kinase (MAPK) pathway, which is involved in various cellular functions including cell proliferation and migration and which can also be activated by TNF or IL-1β (43). Both NF-κB and MAPK pathways share the receptor-associated proteins [such as TNF receptor-associated death domain (TRADD), TNF receptor–associated factor 2 (TRAF2), Receptor interacting protein (RIP)] in their pathways. However, each uses a different intermediate kinase module for signal transduction: IKK module for the NF-κB system and MAPK kinase for the MAPK system

(43). Hence, comparing the activation of these two systems would reveal whether the governing mechanism for the differentiator behavior happens in the shared upstream portion of the signaling cascade or in the divergent downstream portion. To compare the activation profiles in both systems, we applied increasing or randomly fluctuating TNF dose ranging from 0 to 25 ng/ml TNF to cells harboring NF-κB and JNK reporters (Fig. 6, A and B). As observed previously, the NF-κB response corresponded to the dose change from the previous stimulus (correlation coefficient, ~0.84). On the other hand, JNK activity showed little dependence on change in TNF input (showing a correlation coefficient of ~0.36). This result suggests that the differentiator response to the TNF dose change is specific to the NF-κB system and that the governing mechanism lies downstream of the receptor-associated proteins.

If dose differentiation is unique to the NF-κB system, then the next important question would be whether dose differentiation persists in the NF-κB response to other ligands. Many ligands activate canonical NF-κB signaling, including the cytokines secreted by both innate immune effectors and pathogens. We measured the NF-κB response to the dynamics of Pam2CSK4 (Pam), a synthetic diacylated lipopeptide, which mimics bacterial lipoproteins and acts as a Toll-like receptor 2 (TLR2) agonist (Fig. 6C) (44). NF-κB response decreased exponentially when Pam was increased instantaneously, just like it did for TNF and IL-1β. However, when Pam was increased exponentially, the median NF-κB response exhibited a sudden increase around 1 ng/ml and then showed a gradual decrease even as the Pam concentration increased (Fig. 6C), a response not observed for exponential TNF and IL-1β increase. The difference between Pam and TNF/IL-1β persisted even at the single-cell level. When examined with the clustering process used for TNF/IL-1β, the majority of cells in the Pam stimulation exhibited one or two sharp peaks during the entire ramping period (fig. S10). Few cells exhibited robust NF-κB oscillations, and the slope of the fitted lines for each group fluctuated from minus to positive values (0.0021, –0.0095, –0.0481, and 0.0349 for groups 1 to 4, respectively). In contrast, the slopes in the TNF/IL-1β groups were all positive values (0.0373, 0.0515, 0.0585, and 0.0512 for groups 1 to 4 in TNF ramping and 0.0949, 0.0766, 0.0753, and 0.0715 for groups 1 to 4 in IL-1β ramping).

Such a difference in response to dynamic stimulus between Pam and TNF/IL-1β is especially intriguing when considering the similarity and shared components between each pathway. TNF and Pam use different receptor-associated signaling components before converging on the IKK module (43, 45, 46). Thus, it is expected that NF-κB activation dynamics differ between these two signaling pathways. However, IL-1R and TLR2 signaling share an Myd88-dependent pathway and other components downstream of their respective receptors, which makes it unusual that the response to dynamic input is distinct (45, 46). Differences between the IL-1R and TLR2 response have been linked to functional biological outcomes (47, 48), and slight differences in the components between these pathways exist (49), suggesting that there may be previously undefined differences between the TLR2 and IL-1R pathways. It is possible that differences in signal transduction at the level of the receptor may give rise to different functional outcomes, as observed in other receptor-ligand interactions (50). For example, the inactivation or degradation rate of TLR2 may be faster than that of IL-1R because of intrinsic characteristics or additional negative feedback mechanisms. Building this assumption into the simulation reproduced a rapidly declining

NF-κB response for all ramping patterns, especially after strong activation of NF-κB (fig. S11), suggesting that this may be a potential mechanism for the lack of differentiation with Pam.

Dynamic cytokine inputs create distinct NF-κB target gene expression profiles

NF-κB controls the expression of many target genes involved in immunity. To study the implications of NF-κB dose differentiation mechanism on target gene expression, we measured gene expression in cells stimulated with different TNF dynamics. To determine whether NF-κB target gene expression dynamics differed between cytokine dosing patterns, we increased TNF level instantaneously and exponentially to 10 ng/ml in the microfluidic device and retrieved cells at different time points during and after the completion of TNF ramping (Fig. 7, A).

We found that the mRNA expression of NF-κB target genes showed different response patterns under dynamic cytokine input (Fig. 7, B). Some genes closely followed the changes in cytokine concentration and NF-κB dynamic profiles, whereas others showed a tendency for an instantaneous increase in response to a gradual increase in cytokine signal. For example, *A20* and *Ccl2* mRNA levels converged between the two dynamic patterns, with the instantaneous TNF increase resulting in a rapid increase in mRNA, followed by maintenance of a high expression level, whereas mRNA levels under exponential TNF ramping gradually increased in accordance with the increasing NF-κB response. *Ccl2*, which encodes a chemoattractant that recruits sentinel cells to the inflammation site (51), also exhibited an initial sharp peak after instantaneous TNF increase. This pattern, which has been reported previously, may indicate complex temporal dynamics in downstream gene regulation (4). For both genes, when exponential cytokine ramping reached its maximal dose, the mRNA level was similar to the highest mRNA level produced by the instantaneous increase. On the other hand, the expression of *Zfp36* and *Casp4*, which encode proteins that regulate inflammation and facilitate apoptosis (52–54), exhibited minimal up-regulation when TNF was increased exponentially, whereas an instantaneous increase caused a sharp increase in the expression level. These genes were largely unresponsive to a gradual increase in TNF concentration and required a large initial dose for substantial activation.

Serpina3g, which encodes an antiapoptotic factor (55), exhibited a gradual increase at persistent high TNF levels but remained at the basal level when TNF concentration was increased exponentially. *RANTES*, which encodes a leukocyte-recruiting chemoattractant, showed another distinct expression pattern. Regardless of instantaneous or exponential TNF increase, *RANTES* expression continuously increased, and the expression kinetics were similar between the input signal patterns.

DISCUSSION

We showed that during cytokine signaling, the NF-κB pathway accurately reflected the changes in TNF or IL-1β dose rather than the absolute dose itself, in a manner analogous to a differentiator circuit. Using microfluidic live-cell imaging experiments, which enables precise and continuous control of stimulus concentrations over many samples, we found that differentiator behavior occurred in response to various input dynamics, including

instantaneous, linear, and exponential increase, and random fluctuation. However, we also found that NF-κB response did not accurately track dose changes under dynamical Pam stimulation, which suggests that different regulatory and response mechanisms are used upon engagement of different receptors. The lack of Pam dose differentiation is notable, given the similarities in the TLR2 and IL-1R signaling pathways. Both pathways share many important components for NF-κB regulation, including the IKK module and other downstream negative feedback mechanisms. However, IL-1R and TLR2 pathways have been suggested to be phenotypically and functionally different despite the shared signaling components, which is consistent with our results (47, 48). Although the presence of the adaptor protein Toll/IL-1 receptor adaptor proteins (TIRAP) in the receptor-associated complex distinguishes TLR2 from IL-1R signaling, the detailed mechanism for different NF-κB regulation under dynamic Pam stimulation is not clear and will be an interesting question to explore in future work (49). It is unexpected that tracking of longitudinal signaling responses to an evolving stimulus reveals differences in dynamic IL-1β and Pam signaling, which are not otherwise readily observable. Our finding may provide an example of how cells can use shared molecular machinery to distinctively interpret the dynamics of different ligands, as has been previously seen in Notch signaling (50).

We determined that multipoint negative feedback mechanisms mediated by A20 and IκBα store a short-term memory of the previous input level and reset the input transmission, consequently facilitating the differentiator behavior of NF-κB under TNF signals. Furthermore, we demonstrated that the expression profile of NF-κB target genes changes considerably when different input dynamics are applied. Although the final concentrations were the same, some genes (*Zfp36*, *Casp4*, and *Serpina3g*) hardly showed any increase in expression during the increase in cytokine concentration ("input ramping"), whereas the expression of other genes (*A20* and *Ccl2*) corresponded closely to the TNF dose at a given time point during the ramping. These results suggest that cells actively tune their functional response according to signaling input dynamics. The exact role of A20 and IκB genes should be further studied in response to other cytokines, including IL-1β, to determine whether this mechanism is a general feature of NF-κB.

NF-κB localization dynamics have been described in detail previously (18, 56, 57). However, it is still unclear why signaling pathways use these oscillatory responses to immune stimuli, which require complex circuits that are costly to the individual cell. Our study suggests that oscillatory responses can transmit accurate information about the extracellular signaling input dynamics or about how the concentration of the environmental signals change over time. An oscillating circuit involves time domain (frequency) and temporal change in the amplitude. Instead of relying on uncontrolled or natural degradation of signaling intermediaries, which can take from several hours to days, the oscillating circuit can readily respond to input changes from the environment by actively degrading or resetting response regulators. Hence, oscillation itself could provide an optimized platform for measuring dynamic changes in the environmental inputs.

Previous in vivo and in vitro studies showed that during an inflammatory response, TNF and IL-1β molecules accumulate and are degraded at different time scales, each with distinct kinetics (5, 6, 10). How the NF-κB system would process a mixture of

dynamically changing cytokines is still unclear and can be complicated, especially when a distinct cytokine-specific feedback is involved in the signaling pathway (42). A20 mediates signaling cross-talk between TNF and IL-1 because both stimuli strongly induce A20 expression and priming cells with IL-1 reduces their response to subsequent TNF exposures (32, 58). These findings suggest that the differentiation behavior may not be restricted to the same stimulus ("cis-differentiation") but can carry across different stimuli ("trans-differentiation") with respect to the A20 controlled canonical pathway.

In conclusion, our work demonstrates the importance of cytokine dynamics for signal processing and downstream gene expression response in the NF-κB pathway. Cells use multiple negative feedback mechanisms and kinase recycling to repeatedly detect the dynamics of extracellular cytokine accurately. Depending on the dynamic pattern of cytokine increase (instant, linear, or exponential), cells differentially regulate NF-κB target genes so that their expression levels are increased or remain at prestimulus level. Hence, using absolute cytokine levels as the measure of the immune response or diagnosis of immune disease not only is flawed but also may lead to ill-founded conclusions. In addition, our study revealed that the NF-κB response is correlated to the rate of dose change and demonstrated that a biological system can continuously and robustly differentiate the cytokine level in a consistent manner.

MATERIALS AND METHODS

Cell culture

$p65^{-/-}$ NIH/3T3 immortalized mouse embryonic fibroblasts (3T3 cells) harboring p65-DsRed and histone 2B–green fluorescent protein (H2B-GFP) nucleus marker or p65-DsRed, H2B-GFP, and JNK-KTR-mCerulean3 were cultured with Dulbecco's Modified Eagle medium (DMEM; Gibco, 11965092) supplemented with 10% fetal bovine calf serum (HyClone), 1% GlutaMAX (Gibco), and 1× penicillin-streptomycin (Gibco) in a regular flask. 3T3 cells were maintained at 37°C and 5% CO_2. Before reaching 100% confluency, cells were harvested using trypsin-EDTA (Gibco) and diluted ~1:10 in fresh medium for passaging every 2 or 3 days. A20 mutant cells (A20 knockout) built on the basis of thisp65-DsRed 3T3 cells were also cultured and maintained in the same condition. For the experiment, FluoroBrite DMEM (Gibco, A1896702) with the same supplements was used to reduce the background fluorescence.

Microfluidic device design

The previously designed and reported cell culture chip was modified for higher efficiency and success rate (Fig. 1C) (59). The chamber size was increased to 3.5 mm by 0.8 mm to obtain more cells per chamber and images per sample, which improved image analysis and downstream gene expression data collection. The minimum distance between the features was adjusted to 150 μm for robust bonding and easier alignment. The input manifolds and flow pathways were revised for faster flushing between the sample feedings. Our new chip allowed more than 500 cells loaded per chamber and can run 64 independent samples (conditions) in parallel.

Mold fabrication for microfluidic device

The master molds for the new design were fabricated by patterning photoresist deposited on silicon wafer through the multilayer soft lithographic process (59, 60). Briefly, to fabricate the mold for the fluid layer, a positive photoresist (Micro-Chemicals, AZ40XT) was spin-coated on a 4-inch wafer with a spin rate of 3400 rpm to get a feature height of ~25 μm. After developing and hard baking to get the rounded cross-sectional profile, the negative photoresist (Micro-Chemicals, SU-8 3025) was deposited on the top of the AZ layer by spin-coating at 3000 rpm, which produced a feature height of ~30 μm. To fabricate the control layer, SU-8 3025 was spin-coated at 3500 rpm for a feature height of ~25 μm. All exposure of photoresist was done with maskless aligner (Heidelberg, MLA150) using a 375-nm laser and a dose of 280 mJ/cm^2.

Polydimethylsiloxane microfluidic chip fabrication

The two-layer microfluidic chip was made by pouring and curing polydimethylsiloxane (PDMS) (Momentive, RTV-615) on these molds and bonding control and flow layers. PDMS (66 g, 10:1 monomer:catalyst) was poured onto the wafer patterned with flow layer design; air bubbles were removed under vacuum, and the PDMS was cured at 80°C for >5 hours to make a ~2-cm-thick PDMS slab with flow pattern grooved on the bottom. For the control layer, 10 g of PDMS was spun onto the wafer with control pattern at 2200 rpm to achieve a thickness of ~50 μm, which is then cured at 80°C for at least 1 hour. After curing, the flow layer inputs were punched. Both PDMS layers were treated with oxygen plasma (Harrick, PDC-001) and then were aligned using a custom stereomicroscope. The aligned chip was cured at 80°C overnight to allow robust bonding between two layers. The next day, the holes to actuate the control layer were punched; then, the chip was bonded to a glass slide (75 mm by 25 mm by 1 mm) through the same oxygen plasma treatment and baking procedure. Further details of the fabrication process can be found in our previous publication (61).

Microfluidic experiment setup

Before the experiment day, the valves in the control layer of the microfluidic chip were connected to the pneumatic solenoid valves and electronic controller boxes. By actuating different sets of valves, the flow pathway in the microfluidic device could be manipulated either manually or automatically using custom-developed graphic user interface (GUI) (61). Cell chambers in the chip were filled with a 1:3 fibronectin (1 mg/ml) in sterile phosphate-buffered solution (PBS) solution (Sigma-Aldrich, FC010) and incubated overnight at room temperature for thorough coating. On the experiment day, chambers and channels were flushed with fresh medium; then, the microscope box and brick (Life Imaging Services GmbH) that enclose the microfluidic device were set at optimal environment for cell experiment (37°C, 5% CO_2 level, and close to 100% humidity). Cells were concentrated to 5 × 10^6 cells/ml to aim roughly 50% confluency when loaded into the microfluidic chambers. After loading the cells, the chambers were closed for at least 1 hour to allow cells to settle firmly before feeding any medium.

High-throughput automated experiment procedure

The control layer of the microfluidic chip was actuated at 25 to 30 psi for thorough closure of the valves. The opening and closing of the valves were controlled with a custom GUI built with MATLAB (61). The GUI can automate the experimental procedure by running a custom script to improve accuracy, throughput, and reproducibility of the experiment. For each experiment, a new experiment code was written to direct the feeding timing and type of medium fed for each chamber. The media containing different concentrations of TNF-α (Life Technologies, PMC3014), IL-1β (R&D Systems, 401ML010CF), and Pam2CSK4 (InvivoGen, tlrl-pm2s) were prepared right before the experiment and kept on ice during the experiment. All input media were delivered into the chip through polyetheretherketone tubing (VICI, TPK.505) by pressurizing the vials containing the media. Input pressure was minimized (3 to 4 psi) to prevent shear stress on cells during feeding.

Live-cell image acquisition

Phase contrast and epifluorescence images were acquired using Nikon Ti2 microscope enclosed within an incubator system (Life Imaging Services GmbH). Images were captured with 20× magnification through a complementary metal-oxide semiconductor camera (Hamamatsu, ORCA-Flash4.0 V2) and were collected every 5 min. For the p65-DsRed imaging, positions were imaged with 555-nm excitation with 0.5- to 1-s exposure time and 75 to 100% light-emitting diode (LED) intensity (Lumencor, Spectra X), whereas H2B-GFP was imaged under 485-nm excitation light with 50- to 100-ms exposure time and 25 to 50% LED intensity used for nucleus marker (H2B-GFP). We did not notice any sign of photo bleaching even after collecting 150 sets of fluorescence images (equivalent to 12-hour duration experiment). After each experiment, background fluorescence and dark frame images were taken for the flat field correction.

Image analysis

NF-κB response or p65 translocation was assessed by analyzing fluorescence images with custom-developed software (MATLAB). The code first defines the position and boundary of each nucleus using H2B-GFP images. Combining this information across a sequence of images, the trajectory of each nucleus was evaluated (62), which was then combined with p65-DsRed images to get single-cell NF-κB traces. The median nuclear fluorescence was calculated to assess the NF-κB response in each cell. To quantify the background fluorescence for each cell in situ, the 20th percentile of pixel brightness in a small subimage encompassing each cell was evaluated, which was then subtracted from the corresponding p65 measurement. The resulting trace was smoothed using "lowess" method with span size of 5 to reduce the noise from cell movement, collisions between cells, and slight changes in the imaging focus. Using custom-developed analysis software (MATLAB), each cell went through manual inspection to sort out cell death, cell division, or other defects that might affect the data quality. In this study, we inspected ~100,000 cells manually, of which ~30,000 were selected for subsequent data analysis.

Mathematical modeling of NF-κB

To capture the essential mechanism for the differentiation behavior in the NF-κB pathway, a previously published mathematical model was modified and used (4). The details of the mathematical modeling and parameter fitting can be found in Materials and Methods in the Supplementary Materials and tables S1 and S2.

CRISPR-Cas9 gene editing of 3T3 cells

The *A20* gene in *p65⁻/⁻* 3T3 cells harboring p65-DsRed and H2B-GFP was edited through CRISPR-Cas9. A20-targeting guide RNAs (5′-CACCGTTTGCTACGACACTCGGAAC-3′ and 5′-CACCGCTCGGAACTTTAAATTCCGC-3′) were cloned into lentiCRISPR v2 (Addgene Plasmid no. 52961) (63) and used for lentivirus production in human embryonic kidney 293T cells. After 2 days, viral supernatants were collected and concentrated. Infected 3T3 cells were selected with puromycin (2 μg/ml) for 3 to 5 days until cell death subsided. Knockout efficiency was assessed through Western blot (anti-A20: sc-166692, Santa Cruz Biotechnology) (fig. S6).

Cell retrieval from microfluidic device for reverse transcription quantitative polymerase chain reaction analysis

Before the automated experiment was finished, the corner of the microfluidic chip was cut open so that the outlet channel is exposed to air. When finished, cells in the chamber were trypsinized for ~1 min to detach them from surface and then were directed to the open outlet channel by washing the chamber with PBS. The cutting allowed cells to accumulate at the end of outlet channel as a tiny droplet (2 to 3 μl), which can be retrieved easily using a small pipette. The retrieved droplet containing cells were immediately injected into the quantitative polymerase chain reaction (qPCR) tubes containing 5 μl of lysis buffer (provided in CellsDirect Kit) and frozen at −80°C for subsequent NF-κB downstream gene measurements.

Reverse transcription qPCR measurement

Cell lysis, reverse transcription (RT), and preamplification were done using a CellsDirect One-Step RT-qPCR kit (Thermo Fisher Scientific) as previously reported (61). RT-qPCR run with custom (table S3) and predesigned TaqMan probes (catalog no. 4453320 for *Ccl2* and catalog no. 4448892 for *Serpina3g*) on a Bio-Rad CFX384 machine. Cq values calculated using software defaults and normalized to glyceraldehyde-3-phosphate dehydrogenase (GAPDH). Relative expression levels were calculated as $2^{(CqTarget - CqGAPDH)}$.

Supplementary Material

Refer to Web version on PubMed Central for supplementary material.

REFERENCES AND NOTES

1. Hoffmann A, Levchenko A, Scott ML, Baltimore D, The IκB-NF-κB signaling module: Temporal control and selective gene activation. Science 298, 1241–1245 (2002). [PubMed: 12424381]

2. Lane K, Van Valen D, DeFelice MM, Macklin DN, Kudo T, Jaimovich A, Carr A, Meyer T, Pe'er D, Boutet SC, Covert MW, Measuring signaling and RNA-seq in the same cell links gene expression to dynamic patterns of NF-κB activation. Cell Syst. 4, 458–469.e5 (2017). [PubMed: 28396000]

3. Nelson DE, Ihekwaba AEC, Elliott M, Johnson JR, Gibney CA, Foreman BE, Nelson G, See V, Horton CA, Spiller DG, Edwards SW, McDowell HP, Unitt JF, Sullivan E, Grimley R, Benson N, Broomhead D, Kell DB, White MRH, Oscillations in NF-κB signaling control the dynamics of gene expression. Science 306, 704–708 (2004). [PubMed: 15499023]

4. Tay S, Hughey JJ, Lee TK, Lipniacki T, Quake SR, Covert MW, Single-cell NF-κB dynamics reveal digital activation and analogue information processing. Nature 466, 267–271 (2010). [PubMed: 20581820]

5. Hackett T-L, Holloway R, Holgate ST, Warner JA, Dynamics of pro-inflammatory and anti-inflammatory cytokine release during acute inflammation in chronic obstructive pulmonary disease: An ex vivo study. Respir. Res 9, 47 (2008). [PubMed: 18510721]

6. Kiers D, Koch RM, Hamers L, Gerretsen J, Thijs EJM, van Ede L, Riksen NP, Kox M, Pickkers P, Characterization of a model of systemic inflammation in humans in vivo elicited by continuous infusion of endotoxin. Sci. Rep 7, 40149 (2017). [PubMed: 28054645]

7. Nahid MA, Yao B, Dominguez-Gutierrez PR, Kesavalu L, Satoh M, Chan EKL, Regulation of TLR2-mediated tolerance and cross-tolerance through IRAK4 modulation by miR-132 and miR-212. J. Immunol 190, 1250–1263 (2013). [PubMed: 23264652]

8. Rao P, Hayden MS, Long M, Scott ML, West AP, Zhang D, Oeckinghaus A, Lynch C, Hoffmann A, Baltimore D, Ghosh S, IκBβ acts to inhibit and activate gene expression during the inflammatory response. Nature 466, 1115–1119 (2010). [PubMed: 20740013]

9. Tassi S, Carta S, Vené R, Delfino L, Ciriolo MR, Rubartelli A, Pathogen-induced interleukin-1β processing and secretion is regulated by a biphasic redox response. J. Immunol 183, 1456–1462 (2009). [PubMed: 19561107]

10. Xue Q, Lu Y, Eisele MR, Sulistijo ES, Khan N, Fan R, Miller-Jensen K, Analysis of single-cell cytokine secretion reveals a role for paracrine signaling in coordinating macrophage responses to TLR4 stimulation. Sci. Signal 8, ra59 (2015). [PubMed: 26082435]

11. Lacy P, Stow JL, Cytokine release from innate immune cells: Association with diverse membrane trafficking pathways. Blood 118, 9–18 (2011). [PubMed: 21562044]

12. Oyler-Yaniv A, Oyler-Yaniv J, Whitlock BM, Liu Z, Germain RN, Huse M, Altan-Bonnet G, Krichevsky O, A tunable diffusion-consumption mechanism of cytokine propagation enables plasticity in cell-to-cell communication in the immune system. Immunity 46, 609–620 (2017). [PubMed: 28389069]

13. Thurley K, Gerecht D, Friedmann E, Höfer T, Three-dimensional gradients of cytokine signaling between T cells. PLOS Comput. Biol 11, e1004206 (2015). [PubMed: 25923703]

14. Han Q, Bagheri N, Bradshaw EM, Hafler DA, Lauffenburger DA, Love JC, Polyfunctional responses by human T cells result from sequential release of cytokines. Proc. Natl. Acad. Sci. U.S.A 109, 1607–1612 (2012). [PubMed: 22160692]

15. Junkin M, Kaestli AJ, Cheng Z, Jordi C, Albayrak C, Hoffmann A, Tay S, High-content quantification of single-cell immune dynamics. Cell Rep. 15, 411–422 (2016). [PubMed: 27050527]

16. Shirasaki Y, Yamagishi M, Suzuki N, Izawa K, Nakahara A, Mizuno J, Shoji S, Heike T, Harada Y, Nishikomori R, Ohara O, Real-time single-cell imaging of protein secretion. Sci. Rep. 4, 4736 (2014). [PubMed: 24751898]

17. Hoffmann A, Baltimore D, Circuitry of nuclear factor κB signaling. Immunol. Rev 210, 171–186 (2006). [PubMed: 16623771]

18. Mitchell S, Vargas J, Hoffmann A, Signaling via the NFκB system. Wiley Interdiscip. Rev. Syst. Biol. Med 8, 227–241 (2016). [PubMed: 26990581]

19. Cheong R, Bergmann A, Werner SL, Regal J, Hoffmann A, Levchenko A, Transient IκB kinase activity mediates temporal NF-κB dynamics in response to a wide range of tumor necrosis factor-α doses. J. Biol. Chem 281, 2945–2950 (2006). [PubMed: 16321974]

20. Kellogg RA, Tian C, Lipniacki T, Quake SR, Tay S, Digital signaling decouples activation probability and population heterogeneity. eLife 4, e08931 (2015). [PubMed: 26488364]

21. Selimkhanov J, Taylor B, Yao J, Pilko A, Albeck J, Hoffmann A, Tsimring L, Wollman R, Systems biology. Accurate information transmission through dynamic biochemical signaling networks. Science 346, 1370–1373 (2014). [PubMed: 25504722]

22. Adler M, Alon U, Fold-change detection in biological systems. Curr. Opin. Systs Biol 8, 81–89 (2018).

23. Lazova MD, Ahmed T, Bellomo D, Stocker R, Shimizu TS, Response rescaling in bacterial chemotaxis. Proc. Natl. Acad. Sci. U.S.A 108, 13870–13875 (2011). [PubMed: 21808031]

24. Ashall L, Horton CA, Nelson DE, Paszek P, Harper CV, Sillitoe K, Ryan S, Spiller DG, Unitt JF, Broomhead DS, Kell DB, Rand DA, Sée V, White MRH, Pulsatile stimulation determines timing and specificity of NF-κB-dependent transcription. Science 324, 242–246 (2009). [PubMed: 19359585]

25. Lee REC, Walker SR, Savery K, Frank DA, Gaudet S, Fold change of nuclear NF-κB determines TNF-induced transcription in single cells. Mol. Cell 53, 867–879 (2014). [PubMed: 24530305]

26. Zambrano S, De Toma I, Piffer A, Bianchi ME, Agresti A, NF-κB oscillations translate into functionally related patterns of gene expression. eLife 5, e09100 (2016). [PubMed: 26765569]

27. Delhase M, Hayakawa M, Chen Y, Karin M, Positive and negative regulation of IκB kinase activity through IKKβ subunit phosphorylation. Science 284, 309–313 (1999). [PubMed: 10195894]

28. Palkowitsch L, Leidner J, Ghosh S, Marienfeld RB, Phosphorylation of serine 68 in the IκB kinase (IKK)-binding domain of NEMO interferes with the structure of the IKK complex and tumor necrosis factor-α-induced NF-κB activity. J. Biol. Chem 283, 76–86 (2008). [PubMed: 17977820]

29. Behar M, Hoffmann A, Tunable signal processing through a kinase control cycle: The IKK signaling node. Biophys. J 105, 231–241 (2013). [PubMed: 23823243]

30. Catrysse L, Vereecke L, Beyaert R, van Loo G, A20 in inflammation and autoimmunity. Trends Immunol. 35, 22–31 (2014). [PubMed: 24246475]

31. Shembade N, Ma A, Harhaj EW, Inhibition of NF-κB signaling by A20 through disruption of ubiquitin enzyme complexes. Science 327, 1135–1139 (2010). [PubMed: 20185725]

32. Werner SL, Kearns JD, Zadorozhnaya V, Lynch C, O'Dea E, Boldin MP, Ma A, Baltimore D, Hoffmann A, Encoding NF-κB temporal control in response to TNF: Distinct roles for the negative regulators IκBα and A20. Genes Dev. 22, 2093–2101 (2008). [PubMed: 18676814]

33. Werner SL, Barken D, Hoffmann A, Stimulus specificity of gene expression programs determined by temporal control of IKK activity. Science 309, 1857–1861 (2005). [PubMed: 16166517]

34. Zhang Q, Lenardo MJ, Baltimore D, 30 years of NF-κB: A blossoming of relevance to human pathobiology. Cell 168, 37–57 (2017). [PubMed: 28086098]

35. Kellogg RA, Tay S, Noise facilitates transcriptional control under dynamic inputs. Cell 160, 381–392 (2015). [PubMed: 25635454]

36. Lagarias JC, Reeds JA, Wright MH, Wright PE, Convergence properties of the Nelder–Mead simplex method in low dimensions. SIAM J. Optim. 9, 112–147 (1998).

37. Swain PS, Elowitz MB, Siggia ED, Intrinsic and extrinsic contributions to stochasticity in gene expression. Proc. Natl. Acad. Sci. U.S.A 99, 12795–12800 (2002). [PubMed: 12237400]

38. Elowitz MB, Levine AJ, Siggia ED, Swain PS, Stochastic gene expression in a single cell. Science 297, 1183–1186 (2002). [PubMed: 12183631]

39. Lyashenko E, Niepel M, Dixit PD, Lim SK, Sorger PK, Vitkup D, Receptor-based mechanism of relative sensing and cell memory in mammalian signaling networks. eLife 9, e50342 (2020). [PubMed: 31961323]

40. Regot S, Hughey JJ, Bajar BT, Carrasco S, Covert MW, High-sensitivity measurements of multiple kinase activities in live single cells. Cell 157, 1724–1734 (2014). [PubMed: 24949979]

41. Kudo T, Jekni S, Macklin DN, Akhter S, Hughey JJ, Regot S, Covert MW, Live-cell measurements of kinase activity in single cells using translocation reporters. Nat. Protoc 13, 155–169 (2018). [PubMed: 29266096]

42. DeFelice MM, Clark HR, Hughey JJ, Maayan I, Kudo T, Gutschow MV, Covert MW, Regot S, NF-κB signaling dynamics is controlled by a dose-sensing autoregulatory loop. Sci. Signal 12, eaau3568 (2019). [PubMed: 31040261]

43. Sabio G, Davis RJ, TNF and MAP kinase signalling pathways. Semin. Immunol 26, 237–245 (2014). [PubMed: 24647229]

44. Aliprantis AO, Yang RB, Mark MR, Suggett S, Devaux B, Radolf JD, Klimpel GR, Godowski P, Zychlinsky A, Cell activation and apoptosis by bacterial lipoproteins through Toll-like receptor-2. Science 285, 736–739 (1999). [PubMed: 10426996]

45. Boraschi D, Italiani P, Weil S, Martin MU, The family of the interleukin-1 receptors. Immunol. Rev 281, 197–232 (2018). [PubMed: 29248002]

46. Oliveira-Nascimento L, Massari P, Wetzler LM, The role of TLR2 in infection and immunity. Front. Immunol 3, 79 (2012). [PubMed: 22566960]

47. Miller LS, O'Connell RM, Gutierrez MA, Pietras EM, Shahangian A, Gross CE, Thirumala A, Cheung AL, Cheng G, Modlin RL, MyD88 mediates neutrophil recruitment initiated by IL-1R but not TLR2 activation in immunity against Staphylococcus aureus. Immunity 24, 79–91 (2006). [PubMed: 16413925]

48. Chen Z, Su L, Xu Q, Katz J, Michalek SM, Fan M, Feng X, Zhang P, IL-1R/TLR2 through MyD88 divergently modulates osteoclastogenesis through regulation of nuclear factor of activated T cells c1 (NFATc1) and B lymphocyte-induced maturation protein-1 (Blimp1). J. Biol. Chem 290, 30163–30174 (2015). [PubMed: 26483549]

49. Yamamoto M, Sato S, Hemmi H, Sanjo H, Uematsu S, Kaisho T, Hoshino K, Takeuchi O, Kobayashi M, Fujita T, Takeda K, Akira S, Essential role for TIRAP in activation of the signalling cascade shared by TLR2 and TLR4. Nature 420, 324–329 (2002). [PubMed: 12447441]

50. Nandagopal N, Santat LA, LeBon L, Sprinzak D, Bronner ME, Elowitz MB, Dynamic ligand discrimination in the notch signaling pathway. Cell 172, 869–880.e19 (2018). [PubMed: 29398116]

51. Carr MW, Roth SJ, Luther E, Rose SS, Springer TA, Monocyte chemoattractant protein 1 acts as a T-lymphocyte chemoattractant. Proc. Natl. Acad. Sci. U.S.A 91, 3652–3656 (1994). [PubMed: 8170963]

52. Brooks SA, Blackshear PJ, Tristetraprolin (TTP): Interactions with mRNA and proteins, and current thoughts on mechanisms of action. Biochim. Biophys. Acta 1829, 666–679 (2013). [PubMed: 23428348]

53. Casson CN, Yu J, Reyes VM, Taschuk FO, Yadav A, Copenhaver AM, Nguyen HT, Collman RG, Shin S, Human caspase-4 mediates noncanonical inflammasome activation against Gram-negative bacterial pathogens. Proc. Natl. Acad. Sci. U.S.A 112, 6688–6693 (2015). [PubMed: 25964352]

54. Hitomi J, Katayama T, Eguchi Y, Kudo T, Taniguchi M, Koyama Y, Manabe T, Yamagishi S, Bando Y, Imaizumi K, Tsujimoto Y, Tohyama M, Involvement of caspase-4 in endoplasmic reticulum stress-induced apoptosis and Aβ-induced cell death. J. Cell Biol 165, 347–356 (2004). [PubMed: 15123740]

55. Liu N, Wang Y, Ashton-Rickardt PG, Serine protease inhibitor 2A inhibits caspase-independent cell death. FEBS Lett 569, 49–53 (2004). [PubMed: 15225607]

56. Basak S, Behar M, Hoffmann A, Lessons from mathematically modeling the NF-κB pathway. Immunol. Rev 246, 221–238 (2012). [PubMed: 22435558]

57. Hayden MS, Ghosh S, Shared principles in NF-κB signaling. Cell 132, 344–362 (2008). [PubMed: 18267068]

58. Adamson A, Boddington C, Downton P, Rowe W, Bagnall J, Lam C, Maya-Mendoza A, Schmidt L, Harper CV, Spiller DG, Rand DA, Jackson DA, White MRH, Paszek P, Signal transduction controls heterogeneous NF-κB dynamics and target gene expression through cytokine-specific refractory states. Nat. Commun 7, 12057 (2016). [PubMed: 27381163]

59. Gómez-Sjöberg R, Leyrat AA, Pirone DM, Chen CS, Quake SR, Versatile, fully automated, microfluidic cell culture system. Anal. Chem 79, 8557–8563 (2007). [PubMed: 17953452]

60. Unger MA, Chou HP, Thorsen T, Scherer A, Quake SR, Monolithic microfabricated valves and pumps by multilayer soft lithography. Science 288, 113–116 (2000). [PubMed: 10753110]

61. Kellogg RA, Gómez-Sjöberg R, Leyrat AA, Tay S, High-throughput microfluidic single-cell analysis pipeline for studies of signaling dynamics. Nat. Protoc 9, 1713–1726 (2014). [PubMed: 24967621]

62. Crocker JC, Grier DG, Methods of digital video microscopy for colloidal studies. J. Colloid Interface Sci. 179, 298–310 (1996).

63. Sanjana NE, Shalem O, Zhang F, Improved vectors and genome-wide libraries for CRISPR screening. Nat. Methods 11, 783–784 (2014). [PubMed: 25075903]

64. Lu TT, Onizawa M, Hammer GE, Turer EE, Yin Q, Damko E, Agelidis A, Shifrin N, Advincula R, Barrera J, Malynn BA, Wu H, Ma A, Dimerization and ubiquitin mediated recruitment of A20, a complex deubiquitinating enzyme. Immunity 38, 896–905 (2013). [PubMed: 23602765]

65. Mauro C, Pacifico F, Lavorgna A, Mellone S, Iannetti A, Acquaviva R, Formisano S, Vito P, Leonardi A, ABIN-1 binds to NEMO/IKKγ and co-operates with A20 in inhibiting NF-κB. J. Biol. Chem 281, 18482–18488 (2006). [PubMed: 16684768]

66. Skaug B, Chen J, Du F, He J, Ma A, Chen ZJ, Direct, noncatalytic mechanism of IKK inhibition by A20. Mol. Cell 44, 559–571 (2011). [PubMed: 22099304]

67. Tokunaga F, Nishimasu H, Ishitani R, Goto E, Noguchi T, Mio K, Kamei K, Ma A, Iwai K, Nureki O, Specific recognition of linear polyubiquitin by A20 zinc finger 7 is involved in NF-κB regulation. EMBO J. 31, 3856–3870 (2012). [PubMed: 23032187]

68. Zhang SQ, Kovalenko A, Cantarella G, Wallach D, Recruitment of the IKK signalosome to the p55 TNF receptor: RIP and A20 bind to NEMO (IKKγ) upon receptor stimulation. Immunity 12, 301–311 (2000). [PubMed: 10755617]

69. Swanson JA, Lee M, Knapp PE, Cellular dimensions affecting the nucleocytoplasmic volume ratio. J. Cell Biol 115, 941–948 (1991). [PubMed: 1955464]

70. Phelps CB, Sengchanthalangsy LL, Malek S, Ghosh G, Mechanism of κB DNA binding by Rel/NF-κB dimers. J. Biol. Chem 275, 24392–24399 (2000). [PubMed: 10825175]

71. Schwanhäusser B, Busse D, Li N, Dittmar G, Schuchhardt J, Wolf J, Chen W, Selbach M, Global quantification of mammalian gene expression control. Nature 473, 337–342 (2011). [PubMed: 21593866]

72. Mathes E, O'Dea EL, Hoffmann A, Ghosh G, NF-κB dictates the degradation pathway of IκBα. EMBO J. 27, 1357–1367 (2008). [PubMed: 18401342]

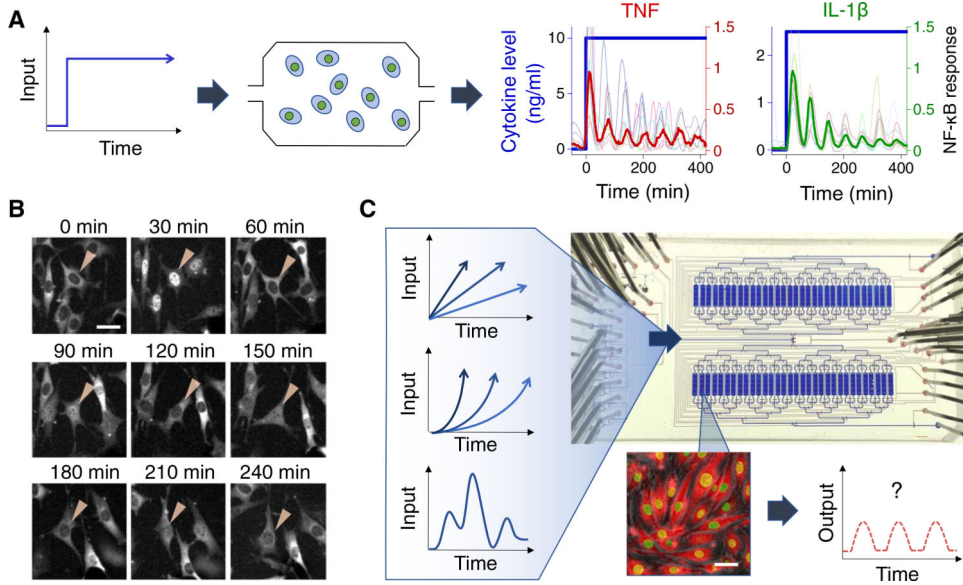**Fig. 1. Single live-cell analysis enables the study of NF-κB response to dynamical signaling inputs.**

(**A** and **B**) Cells were exposed to instantly increase high dose of TNF (red) or IL-1β (green) in a microfluidic device. The thick red or green line indicates the median of single-cell nuclear NF-κB traces, and the thin colored lines represent 10 examples of measured single-cell traces ($N = 150$ cells for each condition). (**C**) To test how NF-κB responds to different input dynamics, cytokine levels (designated as "Input") were increased linearly or exponentially with various rates or doubling times or were introduced in a randomly fluctuating order. Dynamic inputs were introduced to cells expressing p65-DsRed and H2B-GFP through a multiplexed microfluidic cell culture chip. Nuclear NF-κB localization was measured by time-lapse microscopy. White scale bar, 50 μm.
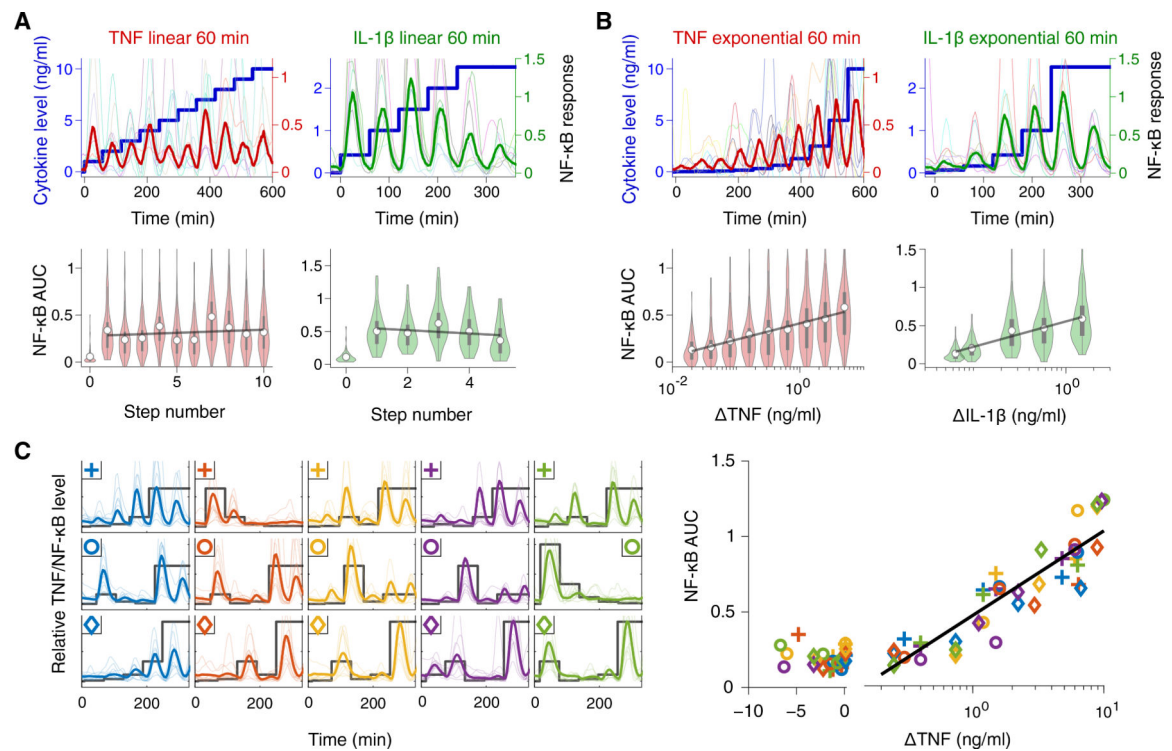
Fig. 2. Dose differentiation by the NF-κB pathway.
(**A** and **B**) TNF and IL-1β concentrations were increased linearly or exponentially at different intervals, and nuclear NF-κB levels were recorded from individual cells. Example single-cell traces from 60-min interval experiments are shown [figs. S1 (B and C) and S2 (B and C) for all TNF intervals]. The thick blue line shows the time-dependent cytokine concentration, and the thick red and green lines show median nuclear NF-κB level during linear (A) ($N = 100$ cells for each test) and exponential (B) ($N = 112$ cells for TNF and $N = 120$ cells for IL-1β) input ramping. Thin lines represent 10 random single-cell traces from each sample. The bottom violin plots show the distribution of NF-κB area under the curve (AUC) at each cytokine dose step, where the white circles represent the mean of single-cell AUCs and the best fit based on differentiator behavior is shown by the thick black thick lines. (**C**) Cells were exposed to variable TNF concentrations in random order. The black line shows TNF input dose ranging from 0 to 10 ng/ml; the thick colored line shows the mean NF-κB trace ($N = 100$ cells for each sample), and the thin lines show 10 random single-cell traces for each sample. On the right scatter plot, the AUC after each dose increase/decrease was calculated and plotted in linear scale for negative TNF (TNF concentration change) and log scale for positive TNF. The black line indicates the best fit to the log function.
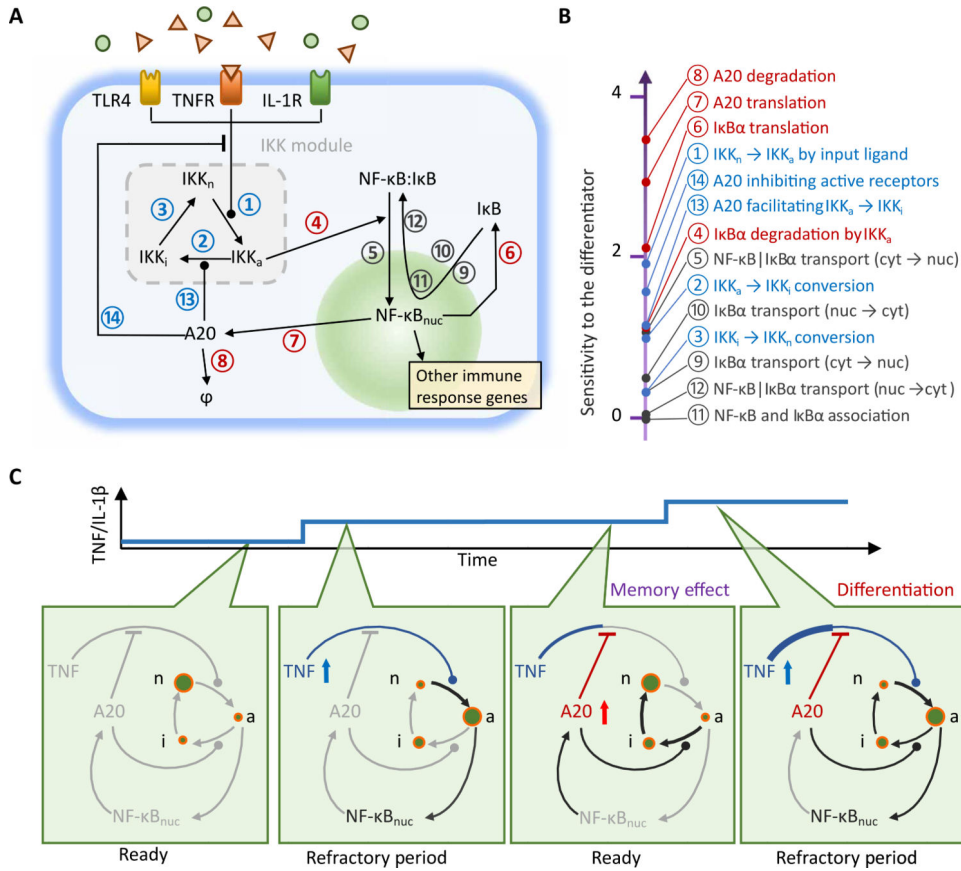
Fig. 3. Computational analysis shows that A20 facilitates dose differentiation by providing memory to NF-κB.

(**A**) The NF-κB circuit describes how cytokine input regulates immune response. Parameters governing cycling dynamics of IKK are in blue; parameters associated with production and degradation of negative feedback molecules (IκBα and A20) are in red, and other parameters used in the sensitivity test are in black. (**B**) For each parameter indicated in (A), the value of the parameter was computationally varied by 10-fold. The change in the statistical distance (χ^2) to the differentiating behavior was calculated (Materials and Methods in the Supplementary Materials), which was used as sensitivity score. More detailed analysis can be found in fig. S4. (**C**) On the basis of the sensitivity test in (B), the schematics of the differentiator mechanism are predicted. Before stimulation with ligand, the system is at the stationary phase with most IKK in the neutral state (IKK_n). Introduction of TNF/IL-1β converts neutral IKK into active form (IKK_a), which triggers the translocation of NF-κB into nucleus (first refractory period). The translocation initiates the production of A20, which inhibits the receptors activated by the ligand and deactivates the active IKK. Here, the amount or activity of A20 depends on the strength or dose of the previous stimulation; A20 thus serves as "memory" of the previous stimulation by dampening the subsequent response. However, if the dose of the ligand is increased, then more receptors become active, overcoming the inhibition by A20. cyt, cytosol; nuc, nuclear.
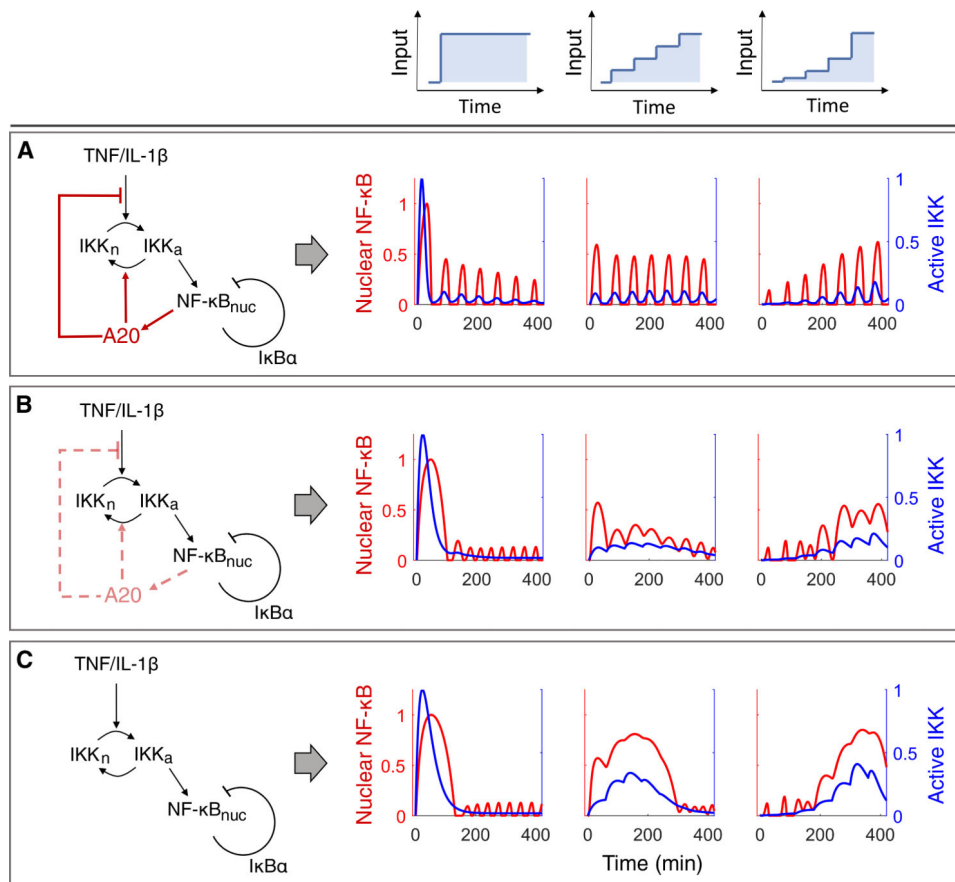
Fig. 4. NF-κB network simulation demonstrates the role of A20 in input differentiation.
(**A**) The red and blue curves represent the dynamics of nuclear NF-κB and active IKK levels under three different input dynamics. The red lines in the circuit diagram highlight the A20 negative feedback, which was investigated in this simulation. (**B** and **C**) The translation rate of A20 is reduced to quarter of the original value (B) or is set to zero (C). The reduced production of A20 undermines the control of upstream signaling through nuclear NF-κB (red dashed line), disrupting the differentiation capability of the system (B). Eliminating negative feedback to upstream components results in greater disruption of the dose differentiation behavior (C).
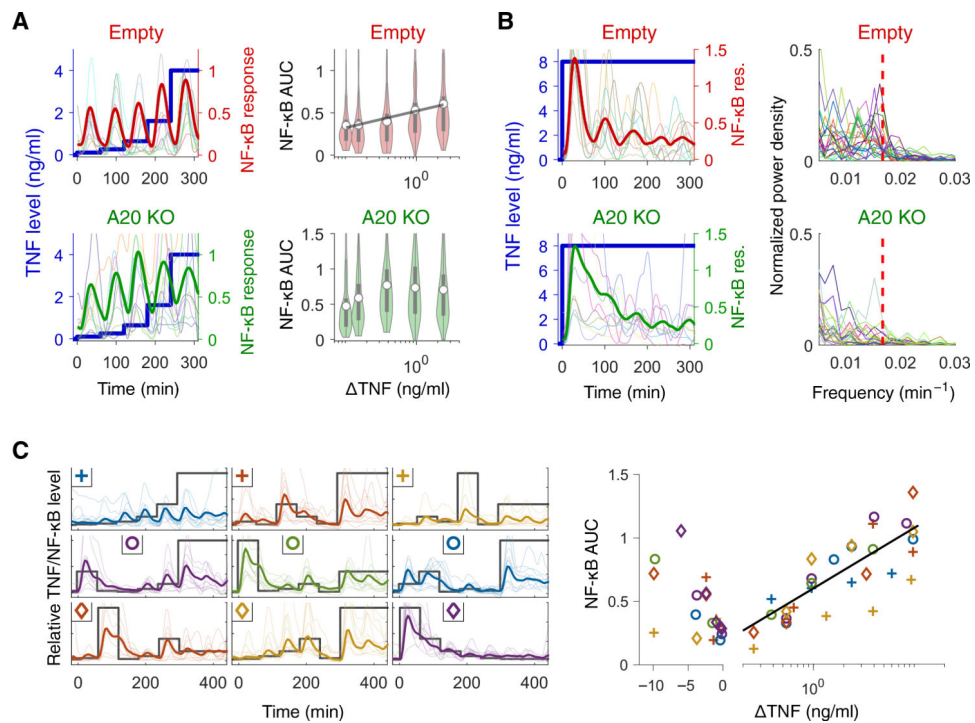
Fig. 5. A20 is critical for sustained input differentiation.
(**A** and **B**) NF-κB translocation was measured in A20 knockout cells (A20 KO) exposed to exponential TNF ramping (A) (*N* = 150 cells for each sample) or instant increase (B) (*N* = 130 cells for each sample). Thin lines represent 10 random single-cell traces from each sample. The results are compared to the wild-type background (Empty). The right violin plots in (A) show the AUC at each time interval, where the white circles indicate the mean of population. For the instant increase in (B), a Fourier transform was applied to each cell trace to evaluate the power density spectrum. (**C**) A20 knockout cells were exposed to doses of TNF fluctuating from 0 to 10 ng/ml in random order (black line). The thick colored line shows the mean NF-κB trace, and the thin lines show 10 random single-cell traces of *N* = 100 cells. On the right scatter plot, AUC after each dose increase/decrease was calculated and then plotted in linear scale for negative TNF (change in TNF concentration) and log scale for positive TNF. The black line indicates the best fit to the log function.
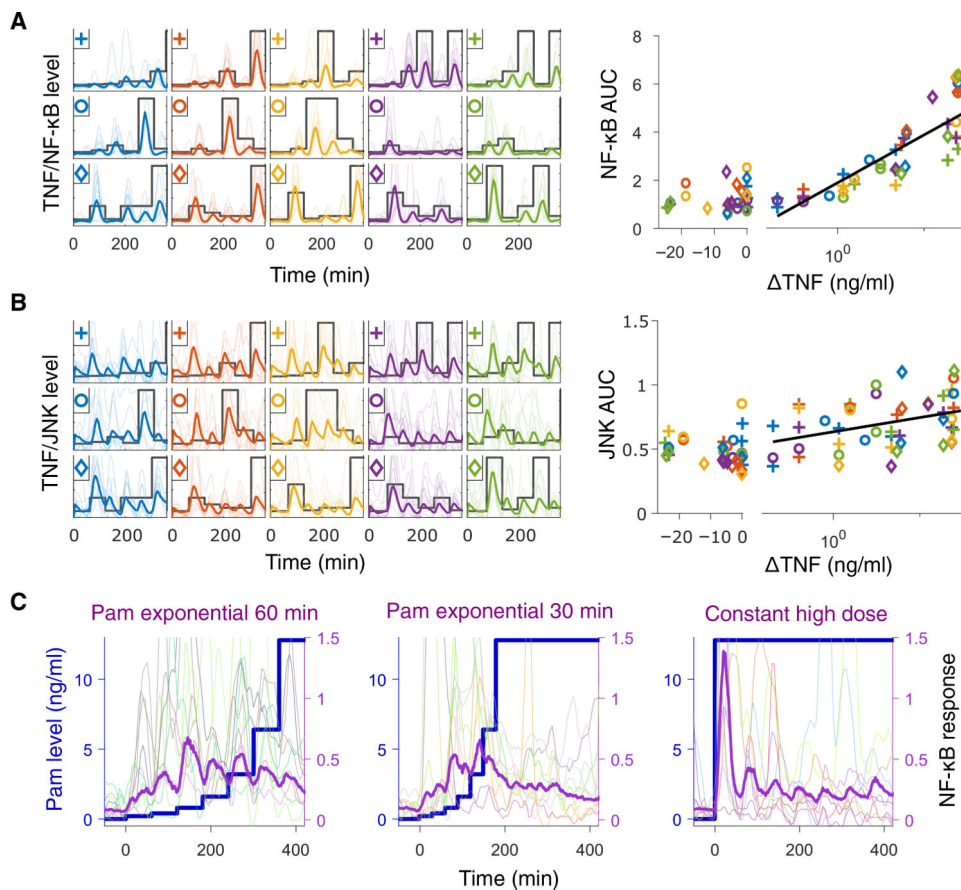
Fig. 6. Input differentiation is specific to the NF-κB system and certain ligand types.
(**A** and **B**) 3T3 cells harboring P65-DsRed and JNK-KTR-mCerulean3 reporters were
exposed to variable TNF concentrations in random order. For both (A) and (B), the black
line shows TNF dose fluctuation ranging from 0 to 25 ng/ml. The top graphs (A) show
the NF-κB response for each dynamic input (10 random single-cell traces from $N = 100$
cells for each subplot), and bottom graphs (B) show the corresponding JNK activity from
the same cells. For both graphs, the thick colored line shows the mean trace, and the thin
lines show 10 random single-cell traces for each sample. The AUC after each dose increase/
decrease and their best fit line to the log function were calculated. (**C**) For exponential
ramping, Pam was doubled every 30 or 60 min from 0.2 to 12.8 ng/ml. For instant increase,
cells were directly exposed to 12.8 ng/ml. Here, the blue lines show the Pam dose, and
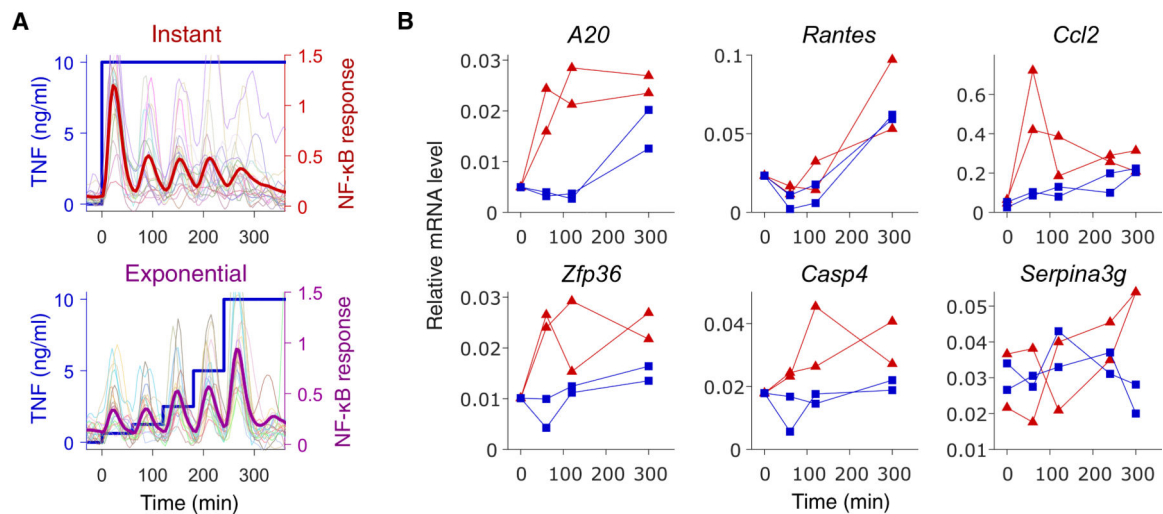purple lines indicate the mean trace of nuclear NF-κB ($N = 140$ cells for each sample).

Fig. 7. NF-κB target genes show distinct expression profiles when stimulated with different TNF dynamics.

(**A**) Cells were stimulated with TNF in two different dynamics: instant increase to 10 ng/ml and exponential increase to 10 ng/ml (twofold increase every hour for 5 hours). To avoid any bias due to the TNF degradation, the chambers in the instant increase sample were also replenished with TNF medium (10 ng/ml) every hour. Thin lines show 20 random traces from $N = 100$ cells for each group. (**B**) At multiple time points during the TNF ramping or constant feeding, cells were retrieved and immediately frozen for subsequent RT-qPCR measurement on NF-κB target genes. The red line shows the gene expression profile from instant increase, and the blue line shows the profile from the exponential ramping. The data points (triangles and squares) are the two biological replicates for each ramping condition.